17. Tommasi, A. and Vauchez, A., *Tectonophysics*, 1997, **279**, 327–350.
18. Vauchez, A., Barruol, G. and Tommasi, A., *Terra Nova*, 1997, **9**, 62–67.
19. Tse, S. T. and Rice, J. R., *J. Geophys. Res.*, 1986, **91**, 9452–9472.
20. Evans, B. and Dresen, G., *Rev. Geophys.*, 1991, **29**, 823–843.
21. Scholz, C. H., *The Mechanics of Earthquakes and Faulting*, Cambridge Univ. Press, 1990, p. 439.
22. Gupta, M. L., *Terrestrial Heat Flow and Geothermal Energy in Asia* (eds Gupta, M. L. and Yamano, M.), Oxford and IBH Pub., 1995, pp. 63–81.
23. Singh, A. P. and Meissner, R., *J. Geodyn.*, 1995, **20**, 111–127.
24. Dube, R. K., Bhayana, J. C. and Chaudhury, H. M., *Pure Appl. Geophys.*, 1979, **109**, 1718–1727.
25. Manglik, A. and Singh, R. N., *Proc. Indian Acad. Sci. (Earth Planet. Sci.)*, 1991, **100**, 389–398.
26. Manglik, A. and Singh, R. N., *Proc. Indian Acad. Sci. (Earth Planet. Sci.)*, 1999, **108**, 15–21.
27. Furlong, K. P. and Fountain, D. M., *J. Geophys. Res.*, 1986, **91**, 8285–8294.
28. Wilks, K. R. and Carter, N. L., *Tectonophysics*, 1990, **182**, 57–77.
29. Verma, R. K. and Banerjee, P., *Tectonophysics*, 1992, **202**, 375–397.
30. Bickle, M. J. and McKenzie, D., *Contrib. Mineral. Petrol.*, 1987, **95**, 384–392.
31. Hoisch, T. D., *J. Geol.*, 1991, **99**, 69–80.
32. Kaila, K. L. and Krishna, V. G., *Curr. Sci.*, 1992, **62**, 117–154.
33. Gupta H. K., Sarma, S. V. S., Harinarayana, T. and Virupakshi, G., *Geophys. Res. Lett.*, 1996, **23**, 1569–1572.
34. Durham, W. B., Mirkovich, V. V. and Heard, H. C., *J. Geophys. Res.*, 1987, **92**, 11615–11634.
35. Ravi Shankar, *Geol. Surv. India Spec. Publ. 10*, 1995, 213–248.
36. Ranalli, G. and Murphy, D. C., *Tectonophysics*, 1987, **132**, 281–295.
37. Kirby, S. H., *Rev. Geophys.*, 1983, **21**, 1458–1487.
38. Hirth, G. and Kohlstedt, D. L., *Earth Planet. Sci. Lett.*, 1996, **144**, 93–110.

ACKNOWLEDGEMENT. We thank the Director, NGRI for his kind permission to publish this work.

Received 28 May 2001; revised accepted 16 October 2001

Cryptic metasomatism in the upper mantle beneath Kutch: Evidence from spinel lherzolite xenoliths

Nitin R. Karmalkar* and Sonal Rege
Department of Geology, University of Pune, Pune 411 007, India

Spinel lherzolite xenoliths entrained in the alkaline rocks from central Kutch vary from fertile (10–12% modal clinopyroxene) to depleted (2–3% modal clinopyroxene) types. Low equilibrium temperatures (884–972°C) indicate entrainment of lherzolite xenoliths from shallow depths within the lithosphere. Variations of major oxides and incompatible elemental concentrations in clinopyroxene indicate a primary control by partial melting. In most of the depleted xenoliths however, the light rare earth elements (LREE), thorium (Th) and niobium (Nb) are strongly enriched and cannot be attributed totally to the process of partial melting. The absence of typical 'metasomatic' minerals, low equilibration temperatures and enriched LREE patterns indicate that the upper mantle below Kutch underwent an event of cryptic metasomatic enrichment prior to partial melting. The distinctive chemical features, viz. LREE enrichment, strong Ti depletion relative to Eu, and slight Nb enrichment, fractionation of Zr and Hf and therefore high Zr/Hf ratio, high La/Yb, Nb/La and low Ti/Eu are all results of interaction of refractory peridotite residues with carbonatite melts.

METASOMATISM is a process in which the chemical composition of the rock is changed by the addition or removal of elements. In the recent years, mantle metasomatism has been invoked to account for the geochemical and isotopic inhomogeneities within the upper mantle documented in peridotite xenoliths entrained in kimberlite and alkali basalts. Although metasomatism in the xenoliths is partly attributed to the transporting magma, most metasomatism takes place before entrainment and is of interest, particularly if its effect can be correlated with coeval and/or later magmatism and tectonic events such as plateau uplift and rifting. Detailed chronological data are, however, needed in this regard.

The appreciation of the fact that metasomatic processes may be important in the upper mantle has led to the terms cryptic and patent metasomatism[1] or modal metasomatism[2] being applied to mantle xenoliths. Patent or modal metasomatism is 'petrographically recognizable due to replacement textures and development of hydrous mineral phases (additional to those commonly seen in peridotites) rich in incompatible elements, replacing anhydrous phases and sometimes associated with the injection of fluids in channel-ways. The more subtle cryptic metasomatism has been proposed for when trace element enrichment occurs in xenoliths, apparently unaccompanied by mineralogical changes.

The alkaline rocks in central Kutch occur as plug, sheet or cone-like intrusions and entrain peridotite xenoliths of mantle origin[3,4]. Prominent plugs occur at Dhrubia, Sayala Devi, Vethon and Dinodhar, whereas sheet-like bodies occur at Bhujia and Lodlai. These rocks are seen intruding the flat-lying or gently-dipping Jurassic sandstones in central Kutch. At Dhrubia, Vethon and Bhujia contact between sandstones and alkaline rocks is concealed by overlying Tertiary limestones or aolian deposits. While in the other localities where the contact is exposed, the Jurassic strata are upturned and exhibit steep dips, or have become silicified near the contact. The mantle xenoliths from Bhujia and Lodlai occur in the central portion

*For correspondence. (e-mail: nrkarmal@unipune.ernet.in)

of the sheet-like intrusion, while those from Dhrubia appear to be concentrated at the lower levels of the plug[4]. The average xenoliths are between 1 and 2 cm, but xenoliths as large as 4–5 cm are common, especially at Bhujia. The xenoliths vary in shape from rounded or subrounded to elongated, and are mostly granular in nature.

Olivine, orthopyroxene, clinopyroxene and spinel in order of abundance dominate the xenoliths. The relatively small size of the xenoliths precludes the determination of precise mineral modes. However, an attempt has been made to determine the average modal abundances by point counting at least 50 samples from different areas. The olivine contents vary between 50 and 60%, opx between 15 and 20%, and cpx between 2 and 13%. The reddish-brown aluminous spinel ranges from 0.5 to 4%.

The spinel peridotites typically are fine-grained (0.5 to 2 mm) and unfoliated, and are type-I (Cr–diopside–spinel) lherzolites[5,6]. They exhibit mostly protogranular[7] or xenomorphic granular[8] microstructures. However, a few samples from the Sayala Devi locality are coarse-grained with weakly-defined planar fabric. Olivine in all samples displays strain shadows and kink bands, and in most samples olivine contains trails of fluid inclusions.

The cpx occurs mostly as discrete grains, smaller than the olivine or opx, and shows finely-spaced exsolution lamellae of opx. The opx in the samples from the Sayala Devi locality contains acicular to prismatic, highly birefringent inclusions, sometimes crossing each other, with oblique extinction. They are too small to analyse, but partial analysis has shown them to be TiO_2-rich, and are similar to the features previously identified as rutile of anomalous habit from the eclogite nodules of the Bultfontain pipe, South Africa and Bargen Arcs, Norway[9]. Exsolved brown platelets of spinel have been observed in the same pyroxenes; the modal abundance of cpx in these samples is very low.

Spinels in the xenoliths are reddish-brown in thin section, and occur in close association with opx and cpx. Volatile bearing phases such as amphibole or phlogopite have not been observed in these xenoliths.

The host basalt infiltrates the xenoliths along grain boundaries. In such cases the olivines and pyroxenes show reaction rims with recrystallization of secondary olivines and pyroxenes or glass. The grain boundaries and intergranular spaces are commonly occupied by a fine aggregate, which microprobe studies have shown to consist of small grains of opx, cpx and olivine set in glass. The spinels also have reacted with this melt, breaking down to a fine-grained aggregate; the relict spinel changes in composition from aluminous to more chromian spinel, while the fine-grained material is titaniferous magnetite.

The glass in the veins intruding the xenoliths is heterogeneous in composition, and mostly silica–alumina or alkali rich.

The clinopyroxene in the xenoliths is chrome–diopside with composition $Wo_{47–49}$ $En_{48–49}$. The cpx has higher Al_2O_3 than the opx (2.5–5.6%); TiO_2 and Al_2O_3 decrease with increasing $Mg^{\#}$. The Al content of cpx decreases with increasing Cr/Cr + Al of spinel, giving an excellent correlation of $Cr^{\#}$ between spinel and cpx. In the suite as a whole (Table 1), the CaO content of cpx is negatively correlated with Al_2O_3 content. In the xenoliths from Dhrubia, high-Al_2O_3 cpx is found in rocks with higher

Table 1. Major element data for Kutch diopsides

	Average cpx core (n = grains)													
Mineral	B1 $n = 6$	B2 $n = 6$	B9 $n = 4$	B22 $n = 5$	D1 $n = 13$	D9 $n = 9$	D12 $n = 7$	SDx2 $n = 5$	SD4 $n = 2$	SD7 $n = 3$	SD17 $n = 7$	DD6 $n = 4$	DD9 $n = 4$	L4 $n = 5$
SiO_2	53.00	52.64	53.00	53.33	52.61	52.51	52.09	52.72	50.71	53.46	53.23	51.50	51.95	52.82
TiO_2	0.12	0.33	0.07	0.08	0.38	0.37	0.26	0.29	1.10	0.68	0.03	0.88	0.46	0.44
Al_2O_3	4.49	5.15	3.97	3.99	5.11	4.49	5.51	5.06	5.06	1.40	2.51	4.87	5.59	3.97
Cr_2O_3	0.74	1.00	1.02	0.85	1.24	0.80	0.88	0.67	0.77	1.16	0.87	0.86	1.15	1.03
FeO	2.34	2.11	2.07	2.87	2.52	2.33	2.81	2.51	2.11	2.74	2.06	2.63	2.29	2.58
MnO	0.07	0.07	0.05	0.09	0.06	0.08	0.08	0.08	0.07	0.07	0.06	0.06	0.04	0.05
MgO	15.33	15.12	15.91	19.49	14.98	15.62	14.54	15.10	15.39	17.14	16.48	15.25	14.36	15.75
CaO	22.48	21.83	22.81	18.24	21.78	23.00	21.88	22.34	23.95	22.67	23.98	23.09	21.96	22.00
Na_2O	1.34	1.67	1.25	0.93	1.76	0.99	1.75	1.43	0.79	0.65	0.64	0.84	1.66	1.26
K_2O	0.00	0.01	0.00	0.00	0.00	0.00	0.01	0.01	0.00	0.05	0.01	0.00	0.01	0.05
NiO	0.05	0.06	0.04	0.04	0.03	0.05	0.04	0.04	0.06	0.00	0.05	0.02	0.07	0.03
Total	99.98	99.97	100.20	99.91	100.48	100.25	99.86	100.25	100.00	100.03	99.91	100.00	99.54	99.97
$Mg^{\#}$	0.921	0.928	0.932	0.924	0.914	0.923	0.902	0.915	0.929	0.918	0.934	0.912	0.918	0.917
Cpx modal	8.10	9.20	7.50	5.10	10.50	5.30	11.50	6.10	2.50	n.a.	3.70	2.70	2.30	0.00
$Cr^{\#}$ cpx	0.176	0.200	0.250	0.216	0.239	0.187	0.171	0.145	0.165	0.517	0.309	0.186	0.211	0.251
$Cr^{\#}$ spinel	0.248	0.317	0.373	0.348	0.335	0.281	0.256	0.208	0.257	0.241	0.527	0.596	0.698	0.460

modal cpx (10.5–11.5%), while low-Al_2O_3 cpx is associated with low modal cpx (5.3%).

The trace element and REE data for the clinopyroxenes are presented in Table 2. Ni, V and Ga contents are negatively correlated with $Mg^{\#}$ and positively correlated with Al_2O_3 content; the same is true of both light and heavy REE. Sc and Co contents show little systematic variation. Primitive-mantle (PM) normalized plots, where the elements are arranged in order of increasing incompatibility from right to left (Figure 1) can be used to group the cpx in three general types. Most samples in the first group have essentially flat patterns, with abundance of the HREE and MREE 2–4 times PM, and the LREE and associated elements showing a spread from 1 to 10 times PM. Some of these samples exhibit negative Ti, Zr and/or Sr anomalies; all have negative Nb anomalies. This group includes most samples from Dhrubia (D), Sayala Devi (SDX) and Dinodhar (DD). A second group shows similar flat HREE–MREE patterns, but is notably enriched in the LREE, Sr, U and Th. All of these samples have negative Ti, Zr and Nb anomalies, but no Sr anomalies. A third group shows a decrease from the HREE to the MREE, and variable enrichment in the LREE, Sr, U and Th. The LREE-enriched samples come especially from the Bhujia locality. On mantle-normalized diagrams, high field strength elements (HFSE) show variable depletions or enrichments. Most of the Kutch diopsides show distinct negative Ti and Zr anomalies. The coexisting orthopyroxene on the other hand, displays slight positive Ti anomalies, consistent with the petrographic observation

Table 2. Trace element data for the Kutch diopsides and the host rock

	Diopsides													
Element	B1	B2	B9	B22	D1	D9	D12	SDX2	SD4	SD7	SD17	DD6	DD9	L4
Th	1.38	1.58	5.93	0.31	0.55	0.19	1.45	0.1	0.08	0.27	0.1	0.24	0.41	7.01
U	1.27	0.38	2.07	0.47	0.16	0.13	0.42	0.1	0.08	0.12	0.7	0.26	0.1	1.92
Nb	0.4	0.96	0.58	0.56	2.66	1.04	1.96	0.34	0.15	3.41	0.28	0.75	1.42	1.37
La	9.57	5.69	39.96	1.08	7.86	2.46	15.49	0.95	1.99	4.89	0.79	3.66	5.8	17.91
Ce	5.75	8.25	66.3	1.24	17.53	6.92	36.17	2.17	7.19	12.67	1.89	10.69	14.03	22.4
Pr	0.36	0.91	4.99	0.18	2.38	1.03	4.7	0.41	1.29	1.9	0.44	1.81	2.02	1.6
Sr	55.16	103.74	435.8	15.28	166.16	49.76	400.17	53.02	36.7	98.35	16.36	111.93	121.7	202.15
Nd	0.96	3.93	12.38	0.94	11.07	5.02	19.27	2.29	7.54	8.87	0.96	9.33	9.59	5.38
Zr	6.41	18.7	4.54	5.46	54.22	26.86	31.58	17.84	61.5	35.96	2.57	51.7	37.51	26.38
Hf	0.32	0.42	0.54	0.53	1.25	0.99	0.83	0.62	2.5	1.2	0.24	1.81	0.92	0.92
Sm	0.36	1.33	1.31	0.5	2.53	1.21	3.25	0.95	2.5	2.64	0.34	2.81	2.4	1.45
Eu	0.19	0.49	0.46	0.29	0.91	0.47	1	0.48	0.9	0.99	0.13	1.07	0.92	0.58
Ti	916.53	2179.17	231.06	594.72	2325.18	2273.34	1611.17	1944.8	7094.11	4716.25	196.05	4821.17	2962.28	2236.19
Gd	0.84	1.78	0.99	0.58	2.96	1.54	2.53	2.09	3.43	3.05	0.38	3.12	2.85	2.29
Dy	1.67	2.54	1.18	1.06	3.06	1.71	2.07	3.22	3.29	4.02	0.51	3.13	3.07	3.12
Ho	0.49	0.64	0.27	0.26	0.67	0.39	0.44	0.76	0.6	0.84	0.12	0.73	0.71	0.7
Y	11.5	15.52	8.77	7.46	16.86	9.95	12.14	19.96	15.62	20.5	2.9	17.31	17.52	18.38
Er	1.36	1.68	0.99	0.98	1.78	1.07	1.29	2.29	1.54	2.38	0.43	1.89	1.82	1.9
Tm	0.23	0.31	0.19	0.16	0.25	0.19	0.19	0.31	0.28	0.35	0.1	0.21	0.26	0.29
Yb	1.5	1.69	0.99	0.8	1.48	1.04	1.33	2.13	1.4	2.18	0.57	1.69	1.52	1.92
Lu	0.23	0.23	0.16	0.16	0.19	0.2	0.21	0.31	0.21	0.26	0.1	0.22	0.23	0.26
Ga	3.19	8.22	3.41	1.72	4	3.26	3.65	4.32	4.11	10.222	2.4	3.73	4.25	3.13
Sc	74.22	87.18	90.69	57.77	78.33	73.77	66.23	77.03	85.57	100.96	78.6	81.5	72.23	77.8
V	266.17	293.77	239.98	202.8	276.36	268.29	276.09	265.85	336.71	423.94	207.13	318.49	267.26	244.17
Co	16.35	19.05	18.46	14.66	17.33	17.73	17.12	16.67	17.87	52.81	16.64	16.65	17.26	15.82
Ni	272.45	335.72	68.97	236.06	275.55	281.92	294.12	259,79	217.52	760.72	280.26	273.38	251.57	265.34
Ti/Eu	4823.842	4447.286	502.3043	2050.759	2555.143	4836.894	1611.17	4051.667	7882.344	4763.889	1508.077	4505.766	3219.87	3855.5
La/Yb	4.417341	2.331126	27.9467	0.934704	3.677063	1.637729	8.063806	0.308805	0.984159	1.553076	0.959605	1.499459	2.641951	6.458544
Zr/Hf	20.05	44.05	8.3613	10.2495	43.2662	27.1718	38.1862	28.596	24.5842	29.99	10.65	28.64	40.81	28.61
Y/Ho	23.46939	24.25	32.48148	28.69231	25.16418	25.51282	27.59091	26.26316	26.03333	24.40476	24.16667	23.71233	24.67606	26.25714
Ti/Nb	2276.53	2274.71	396.7325	1061.991	875.1145	2193.07	824.1284	5704.89	45976.09	1381.85	694.96	6471.36	2081.72	1628.33
Y/Ho	23.46939	24.25	32.48148	28.69231	25.16418	25.51282	27.59091	26.26316	26.03333	24.40476	24.16667	23.71233	24.67606	26.25714
Ti/Nb	2276.53	2274.71	396.7325	1061.991	875.1145	2193.07	824.1284	5704.89	45976.09	1381.85	694.96	6471.36	2081.72	1628.33

Host rock	b	bh	d7	dd	L1	n	na	sd	v
Nb/Ta	17.2117	15.84906	15.77181	15.32847	17.03854	17.44966	17.48252	15.5102	16.71233
Y/Ho	28.86598	28.91566	29.48718	29.41176	29.54545	28.73563	27.38095	27.90698	28.45528
Zr/Nb	2.9	5.142857	4.574468	5.095238	3.297619	4.096154	3.62	5.289474	4.52459
Zr/Hf	45.83333	45.08197	47.59825	43.85246	46.07843	46.55172	44.85294	44.88017	46.6129
Ti/Eu	5278.387	6149.42	6850.457	6211.111	6444.105	7151.77	7289.64	8318.412	8178.939

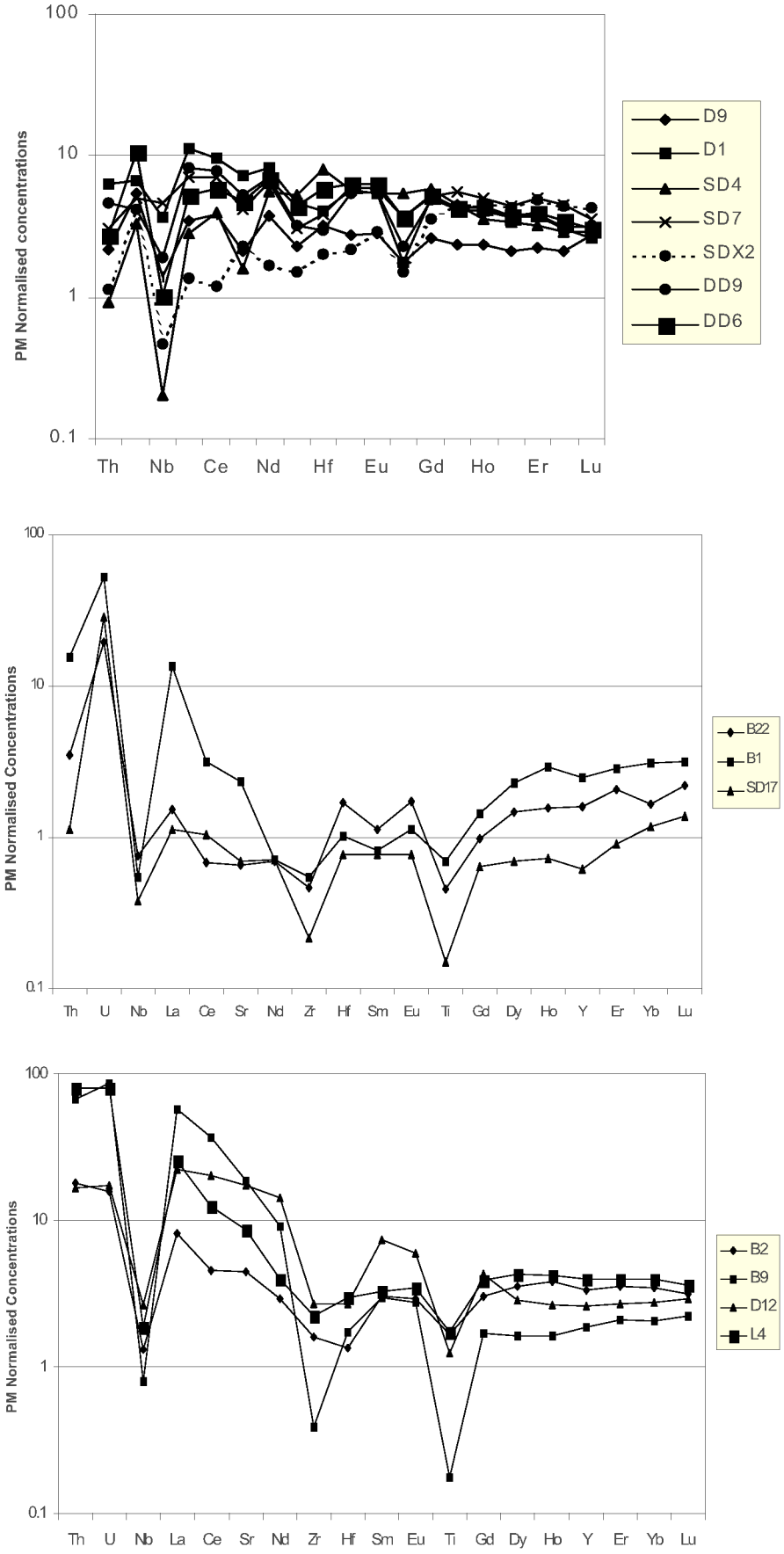

Figure 1. Trace element patterns in cpx.

of rutile exsolution in some samples. However, calculations based on the measured modes show that the observed positive Ti anomaly is not sufficient to balance the strong negative anomaly for Ti observed in many of the Cr-diopsides[10]. Ti is depleted relative to Eu in all samples, whereas Zr and Hf may or may not be depleted when compared with Sm. Nb is depleted compared to La in all the samples. Most of the diopsides show negative Nb anomalies; however, even in the samples with the deepest Nb anomalies, more Nb is present than would be expected from the simple melt extraction model. This suggests that either Nb has been added to cpx during metasomatism, or that the adopted value of D_{Nb} is not appropriate. There is no phase present in the sample that can balance the observed Nb anomaly. The ratios of Zr/Hf and Y/Ho in the Kutch diopsides vary from near chondritic to a high value.

It is generally believed that ratios of Zr/Hf, Y/Ho and Nb/Ta in basalts and peridotites do not get fractionated and are near chondritic. This is because these pairs are considered 'geochemical twins' due to their similar geochemical behaviour as a result of their identical ionic radii and charge, and hence similar partition coefficients. Recent studies, however, have demonstrated that these elements may get fractionated by H_2O-, CO_2- and/or fluorine-rich metasomatizing fluids or melts migrating through the mantle[11,12]. The Zr/Hf ratios in the Kutch diopsides exhibit a wide range, while on the contrary the Y/Ho ratios do not differ significantly from the chondritic value as is true for large number of peridotites, as can be seen in the published literature. We have no data on the Nb/Ta ratio in the Kutch diopsides, however, the Nb/Ta ratio for the host basalts exhibits limited variation, the Y/Ho ratio is near chondritic, while the Zr/Hf ratio in the basalts follows the diopside trend.

The depletion of Al, Ti, Ga, Y and the HREE with increasing $Mg^{\#}$ in diopside, the increase in Ni and Ni/Co with increasing $Mg^{\#}$ in olivine, and the associated increase in Cr/Al of spinels are all the characteristics expected for progressive extraction of partial melt from the mantle. The extreme concentrations of incompatible elements, including the LREE in the Kutch xenoliths require a source, which is highly enriched. The trace-element patterns of the clinopyroxenes have been used to model the melting conditions in intraplate mantle-derived xenoliths[13,14]. The more compatible elements such as Y and Yb have been used in these studies to avoid problems associated with the possible metasomatic mobility of Ti and Zr. The elements Y and Yb were similarly modelled from the clinopyroxenes of the Kutch xenoliths, the details of which have been discussed elsewhere[10]. Batch melting and fractional melting are considered separately, although for small degrees of melting there is a little difference in the resulting composition. A degree of melting is estimated by comparison of the analysed sample with the modelled pyroxenes. The Y and Yb concentrations for the Kutch diopsides follow the predicted melting trends, with only 2 to 5% melting of primitive mantle source being necessary to produce the concentrations observed in the more fertile samples[10]. It is observed that although the majority of the HREE concentrations can be explained by low degrees of partial melting of the source material, the MREE and LREE concentrations are higher than those predicted for the residues of partial melting. The trace-element patterns observed in most of the diopsides from the Kutch region thus cannot be explained by partial melting processes alone, and require the addition of incompatible components to clinopyroxenes previously depleted by partial melting.

Numerous recent studies have emphasized the importance of metasomatism as precursor to the alkaline magmatism. 'Mantle metasomatism', is a term used for all additions or removals of chemical components by means of melts or fluids, or by diffusive exchange. Experimental and petrographic studies have indicated that this metasomatic fluid could be silicate or carbonatitic in composition[15,16] and would carry the necessary inventory of incompatible trace elements. Carbonatite melts have very low viscosities and may be effective agents for transporting incompatible elements in the upper mantle and thus are important in controlling the incompatible trace element budget in the lithospheric mantle. The REE compositions of these peridotites do not directly reflect the composition of the metasomatizing melt/fluid. In the present case the clinopyroxene will be the main host of the REE and the bulk partition coefficients can be calculated from their modal abundances. Comparing the present data set with the published work[17] for the Olmani peridotites of Tanzania and that for the mantle xenoliths of eastern Australia[13] indicates that the coexisting melt was LREE-enriched. The metasomatic process has enriched the diopsides in Th, U, Nb, Sr, Zr and LREE (La–Eu) and has fractionated Zr from Hf, leading to some unusually high Zr/Hf ratios (samples D1, D12, DD9; Table 1) similar to a number of erupted East African carbonatites. The inverse relationship observed between $Mg^{\#}$ and Ce content suggests that the addition of these elements has been accompanied by addition of Fe.

Invasion of peridotitic mantle by low-viscosity carbonatitic or hydrous alkaline melts leads to modal or cryptic metasomatism[1,2] in which a range of accessory phases such as amphibole, phlogopite, apatite, zircon, etc. can host otherwise highly incompatible elements. Presence of these mineral phases not only results in an absolute increase in certain highly incompatible elements, but also leads to fractionation of certain incompatible trace element ratios. The ratios Nb/Ta and Zr/Hf, for example, get highly fractionated. No volatile-bearing phases such as amphibole, phlogopite or apatite have been observed in the samples studied, and hence these samples can be said to be cryptically metasomatized[1], this may suggest that the inferred metasomatic fluids were low in water content.

The distinctive HFSE fractionations relative to the REE in the Olmani peridotite, Tanzania have been thought to reflect both clinopyroxene-melt partitioning and the characteristics of metasomatizing melt of carbonatitic composition[17]. The partition coefficients for elements Ti, Zr, P and K are such that the incipient carbonatite melt gets depleted in these elements relative to a silicate melt[18], while Nb and Sr get enriched, and will impose this characteristic on metasomatized peridotite. Ti partition coefficients for clinopyroxene in equilibrium with carbonatitic magmas suggest that Ti enters the clinopyroxene in preference to Eu[17]. Thus if the liquid with which the Kutch diopsides reacted was carbonatite, the diopsides before reacting had an even greater Ti depletion relative to Eu than that currently exhibited by Kutch diopsides. Figure 1 show that the fluids were capable of adding Nb and Zr, but apparently did not affect the Ti contents of cpx significantly, leading to very low values of Ti/Nb. Low Ti/Nb ratios may also reflect carbonatitic metasomatism[13]. Enrichment in Nb has been interpreted as evidence against the role of water or hydrous fluids as the metasomatic agent, based on the low solubility of Nb in such fluids[19]. Strong Zr, Hf and Ti depletions and Nb enrichments relative to the REE, and high Zr/Hf ratios are characteristic of many erupted carbonatites[11,20]. This has been attributed to fractionation and removal of potential carriers of HFSE such as sphene, niobian perovskite or zircon[20]. It has been shown that Nb partitions strongly into a carbonatite melt coexisting with a silicate melt[21]. Experimental data on the partitioning behaviour of the trace elements demonstrate that primary carbonatites will be depleted in Ti relative to the middle REE[18]. Hence we envisage that the HFSE fractionation patterns in the Kutch diopsides reflect the characteristics of the metasomatizing carbonatite melt. This melt was strongly enriched in the LREE content, had low Ti/Eu, high Nb/La and fractionated Zr/Hf. The Zr/Hf ratio of three samples is anomalously high (D1, D12, DD9), and this anomalous Zr/Hf ratio has been suggested as one of the signatures of carbonate-related mantle metasomatism[11]. Hf is believed to be partitioned more strongly into the silicate melt than Zr, leading to higher Zr/Hf ratios in a coexisting carbonate melt[22].

Sr enrichment has been regarded as the consequence of trace element exchange between a carbonatite medium and peridotite minerals such as clinopyroxenes[23]. Although no carbonate has been observed in the samples, glass patches are common, and the glass is generally enriched in silica alumina or alkalis; such glasses have been interpreted as the product of reaction between mantle rocks and carbonate-rich fluids[24].

The nature of the carbonate melt at upper mantle pressures has wider implications within the context of mantle metasomatism. It has been suggested that due to their high separation velocities, low viscosities[25] and high diffusivities, carbonatite magmas could be effective agents of chemical transport within the upper mantle. Many recent studies have documented evidence for the interaction of carbonatite melts with peridotite xenoliths[13,17,26,27]. Minerals such as pargasitic amphibole, apatite and the clinopyroxene-enriched character of the SE Australian xenoliths have been shown to be the consequence of the carbonatitic metasomatism[27]. The geochemical characteristics of mantle-derived carbonatite include high La/Yb, Zr/Hf and Ca/Al ratios and low Ti/Eu ratios. It has been pointed out that these ratios are not individually unique to carbonatite melts, but together provide evidence for carbonatite metasomatism[17]. Comparison of natural carbonatite compositions[20] with silicate melt compositions such as OIB[28] shows carbonatites to be enriched in La, Ce and Sr and depleted in Hf and Ti. Thus the work on the natural samples (carbonated peridotites) consistently predicts high LREE/HREE, LREE/Hf and Sr/Hf ratios and low Ti/Sr and Ti/REE ratios in mantle mineralogies residual to carbonatite interactions[18].

Carbonatites are rare igneous rocks and isotopic studies have indicated a mantle source for carbonatitic magmas. These primary carbonatite melts form on the high-pressure side of the thermal maximum, or 'ledge' in the solidus for fertile peridotite $CO_2 \pm H_2O$ and, on ascent these liquids will be eliminated by reaction. They may remain in equilibrium with their mantle host according to the reaction:

$$\underset{\text{dolomite}}{CaMg(CO_3)_2} + \underset{\text{orthopyroxene}}{4MgSiO_3} = \underset{\text{clinopyroxene}}{CaMgSi_2O_6} + \underset{\text{olivine}}{2Mg_2SiO_4} + \underset{\text{fluid}}{2CO_2}$$

Such carbonatitic melts have generally been regarded as 'ephemeral'. In intraplate regions the nature of peridotite–CO_2–H_2O solidi are such that upward percolation of low-melt fraction, carbonated silicate melt may lead to lithospheric metasomatism above ~ 90 km (30 kbar). The above reaction produces metasomatic clinopyroxene at the expense of orthopyroxene, changing lherzolite to wehrlite. Equilibration of magnesian carbonatite melts with wehrlite at pressure lower than that of solidus 'ledge' (i.e. < 2.5 Gpa) changes the carbonatite melt to more calcic compositions[29,30]. Once the channel-ways with wehrlite reaction are established in the upper mantle, carbonate melts are able to survive and ascend into the crust[31,32]. Ascent rates from fluid flow calculations have been estimated at 20–65 m/s (ref. 32). Calculated temperatures and pressures of equilibrations for the Kutch xenoliths (~ 950°C; ~ 10–20 kbar) indicate that this metasomatism is likely to have occurred within the sub-continental lithospheric plate, at a depth immediately above the CO_2–H_2O–peridotite solidus ledge. In contrast to the examples discussed[27], however, the metasomatism that enriched the Kutch xenoliths does not seem to have produced cpx-enriched wehrlites, perhaps because of the low fluid/rock ratio.

It has been demonstrated[16] that addition of very small amounts of carbonatite melt has a dramatic effect on both

P_2O_5/TiO_2 and LREE enrichment in peridotitic residues. Geochemical features characteristic of mantle-derived carbonatite melts have been documented[17]. These include high La/Yb, very high Zr/Hf, very low Ti/Eu and high Ca/Al. Bulk mixing of carbonatite melts with that of the refractory peridotite has been advocated on the basis of decarbonation reactions that occur when carbonatite melt enters a peridotite[17]. Following this model we have plotted the degree of Ti depletion against the degree of LREE enrichment (Figure 2 *a*) in the diopsides from Kutch xenoliths, and also the composition of diopsides from SE Australia[13]. The entire data set exhibits a negative correlation; this has been interpreted as the product of mixing of a small amount of carbonatite melt. A possible test of this model is to determine whether peridotites with low Ti/Eu have higher modal clinopyroxene content, which would be expected if these geochemical features were related to addition of Ca-carbonatite magma[17]. As previously stated, the relatively small size of the xenoliths precludes the determination of precise mineral modes. However, the measured modal content of the diopsides does correlate negatively with that of Ti/Eu (Figure 2 *b*), supporting the Ca-rich nature of the carbonatite fluid/magma.

As we do not have the isotopic data on these xenoliths, the exact timing of the metasomatic event cannot be established. However, based on the chemical characteristics of both the xenoliths and the host basalt and the textural

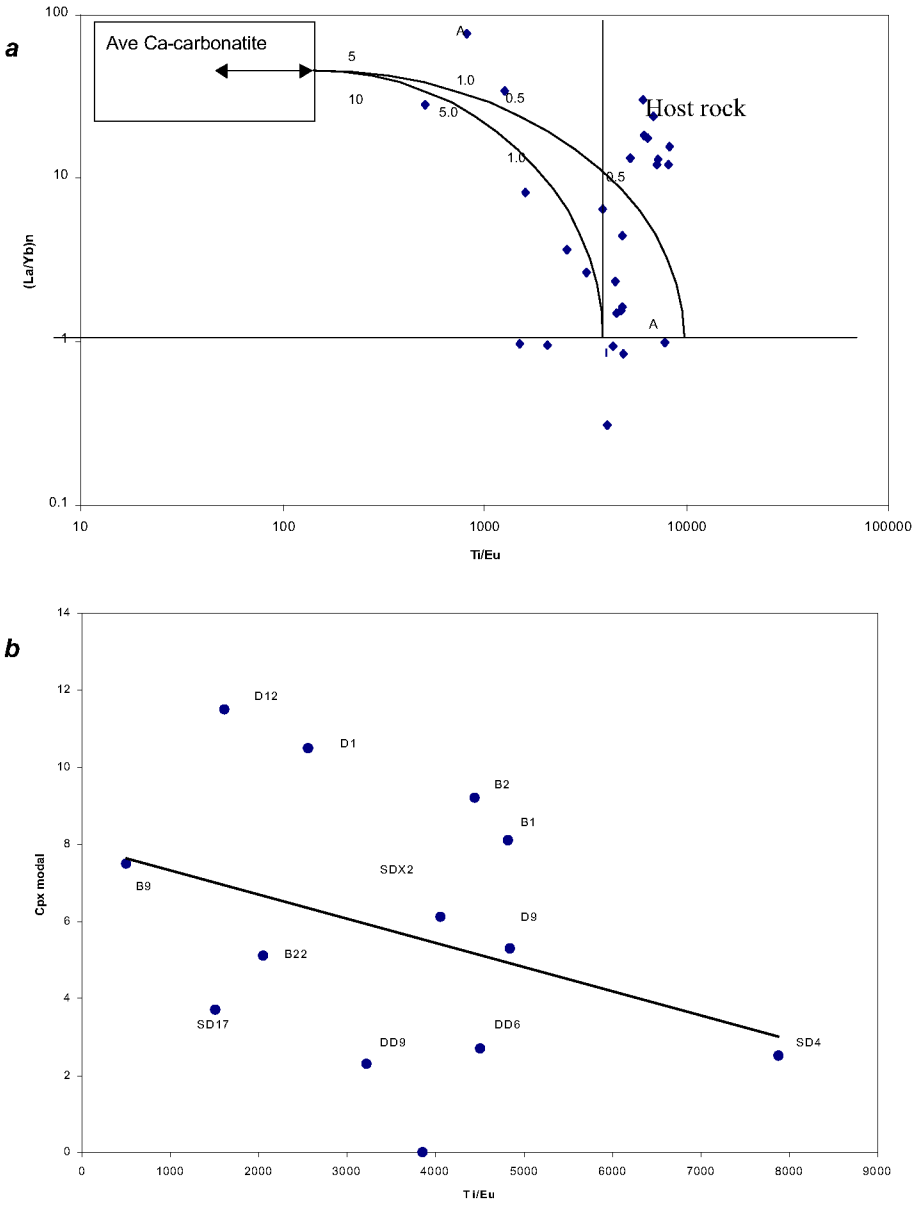

Figure 2. ***a***, Ti/Eu vs PM normalized La/Yb ratio for the Kutch xenoliths; and those from SE Australia [A]; ***b***, Ti/Eu vs modal diopside content in the Kutch xenoliths.

characters of the xenoliths, certain inferences can be drawn.

The individual primary minerals in the xenoliths are in textural equilibrium. The individual mineral grains in all the Kutch xenoliths analysed are unzoned with respect to trace elements, indicating pervasive homogenization of the metasomatic signature. Hence the enrichment is an upper-mantle event and cannot be linked to the magmatism that brought them to the surface. This implies that a metasomatic fluid interacted with the peridotite at relatively low temperatures in the lithospheric mantle[33]. The calculated temperature–pressure conditions support this contention.

When the host-rock data are compared with the xenoliths data, it is observed that the rock samples have very low values for Ti/Eu ratio coupled with negative Zr anomaly, fractionated Zr/Hf ratio, Sr, Ba and Nb enrichment, the characters consistent with their derivation from source which has experienced carbonatite metasomatism. The data for the host rock have also been plotted along with the xenolith data and they fall on the line of carbonatite metasomatic trend[17].

Addition of Nb along with the other highly incompatible trace elements appears to be inconsistent with an arc-related hydrous fluid or brine, as the HFSE are essentially unaffected by subduction-related fluxes into arc magmas[34]. Nb is immobile in such fluids[19]. This indicates enrichment of the Kutch xenoliths in an intraplate setting, either within continental lithosphere or in association with mantle plume. Ratios of highly incompatible elements of both the alkaline rocks and the entrained mantle xenoliths in the present study clearly support the role played by the plume in metasomatizing the lithospheric mantle. Thus the observed trace element variation of the alkaline rocks is indicative of the fact that the alkaline magmatism in Kutch is formed as a consequence of melting of such metasomatized, subcontinental, lithospheric mantle. The metasomatic event hence seems to be at least older than the alkaline activity in the Kutch area. The metasomatic activity can be attributed to the alkaline melts or fluid derived from the upwelling Reunion plume at the time of continental break-up. Recently a low-velocity anomaly has been delineated to the north of Cambay Gulf on the basis of seismic studies[35]. This feature is 120 km across, and the centre of this anomaly lies just below Mer-Mundwara and Sarnu-Dandali alkaline complexes in western Rajasthan. The low-velocity feature may probably represent a fossil expression of the Deccan plume. The alkaline magmatism in the areas of Mer-Mundwara and Sarnu-Dandali as well as that from the Kutch region has been related to the plume activity[36,37]. It is worthwhile mentioning that the Kutch region is not far away from this low-velocity zone.

1. Dawson, J. B., in *Kimberlites II* (ed. Kornprobst, J.), Elsevier, Amsterdam, 1984, pp. 289–294.
2. Harte, B., in *Continental Basalts and Mantle Xenoliths* (eds Hawkesworth, C. J. and Norry, M. J.) Shiva, Natwich, 1983, pp. 46–91.
3. De, Aniruddha, Report of 22nd Session of Int. Geol. Cong., New Delhi, Part III, 1964, pp. 126–138.
4. Krishnamurthy, P., Pande, K., Gopalan, K. and Macdougall, J. D., *Geol. Soc. India, Spl. Publ.*, 1989, **10**, 53–68.
5. Wilshire, H. G. and Shervais, J. W., *Phys. Chem. Earth*, 1975, **9**, 257–272.
6. Frey, F. A. and Prinz, M., *Earth Planet. Sci. Lett.*, 1978, **38**, 129–176.
7. Mercier, J. C. and Nicolas, A., *J. Petrol.*, 1975, **16**, 454–487.
8. Harte, B., *J. Geol.*, 1977, **85**, 279–288.
9. Griffin, W. L., Jensen, B. B. and Misra, S. N., *Nor. Geol. Tidsskr.*, 1971, **51**, 177–185.
10. Karmalkar, N. R., Griffin, W. L. and O'Reilly, S. Y., *Int. Geol. Rev.*, 2000, **42**, 416–444.
11. Dupuy, C., Liotard, J. M. and Dostal, J., *Geochim. Cosmochim. Acta*, 1992, **56**, 2417–2423.
12. Green, T. H., *Chem. Geol.*, 1995, **120**, 347–359.
13. Norman, M. D., *Contrib. Mineral. Petrol.*, 1998, **130**, 240–255.
14. Xu, X., O'Reilly, S. Y., Griffin, W. L. and Zhou, X., *J. Petrol.*, 2000, **41**, 111–148.
15. Green, D. H. and Wallace, M. E., *Nature*, 1988, **336**, 459–462.
16. Baker, M. B. and Wyllie, P. J., *Geochim. Cosmochim. Acta*, 1992, **56**, 3409–3422.
17. Rudnick, R. L., McDonough, W. F. and Chappell, B. C., *Earth Planet. Sci. Lett.*, 1993, **114**, 463–475.
18. Sweeney, R. J., Prozesky, V. and Przbylowicz, W., *Geochim. Cosmochim. Acta*, 1995, **59**, 3671–3683.
19. Keppler, H., *Nature*, 1996, **380**, 237–239.
20. Nelson, D. R., Chivas, A. R., Chappel, B. W. and McCulloch, M. T., *Geochim. Cosmochim. Acta*, 1988, **52**, 1–17.
21. Green, T. H., Adam, J. and Sie, S. H., *Contrib. Mineral. Petrol.*, 1992, **46**, 179–184.
22. Hamilton, D. L., Bedson, P. and Eson, J., in *Carbonatites: Genesis and Evolution* (ed. Bell, K.), Unwyn Hyman, London, 1989, pp. 405–427.
23. Ionov, D. A., Dupuy, C., O'Reilly, S. Y., Kopylova, M. G. and Genshaft, Y. S., *Earth Planet. Sci. Lett.*, 1993, **119**, 283–297.
24. Ionov, D. A., Hoffman, A. W. and Shimizu, N., *J. Petrol.*, 1994, **35**, 753–785.
25. Watson, E. B., Brenan, J. M. and Baker, D. R., in *Continental Mantle* (ed. Menzies, M. A.), Oxford Univ. Press, 1991, pp. 111–126.
26. Hauri, E. H., Schimizu, N., Dieu, J. J. and Hart, S. R., *Nature*, 1993, **365**, 221–227.
27. Yaxley, G. M., Crawford, A. J. and Green, D. H., *Earth Planet. Sci. Lett.*, 1991, **107**, 305–317.
28. Sun, S. S. and McDonough, W. F., in Magmatism in the Ocean Basins (eds Saunders, A. D. and Norry, M. J.), Geol. Soc. Spl. Publ., 1989, vol. 42, pp. 313–345.
29. Dalton, J. A. and Wood, B. J., *Earth Planet. Sci. Lett.*, 1993, **119**, 511–523.
30. Sweeney, R. J., *ibid*, 1994, **128**, 259–270.
31. Harmer, R. E. and Gittins, J., *J. Afr. Earth Sci.*, 1997, **25**, 5–28; *J. Petrol.*, 1988, **39**, 1895–1903.
32. Genge, M. J., Price, D. and Jones, A. P., *Earth Planet. Sci. Lett.*, 1995, **131**, 225–238.
33. Witt-Eickschen, G. and Kramm, U., *J. Petrol.*, 1997, **38**, 479–493.
34. Pearce, J. A., Baker, P. E., Harvey, P. K. and Luff, I. W., *ibid*, 1995, **36**, 1073–1109.
35. Kennet, B. I. W. and Widivantro, S., *Earth Planet. Sci. Lett.*, 1999, **165**, 145–156.
36. Basu, A. R., Renne, P. R., Dasgupta, D. K., Teichmann, F. and Poreda, R. J., *Science*, 1993, **261**, 902–906.

37. Simonetti, A., Goldstein, S. L., Schmidberger, S. S. and Viladkar, S. G., *J. Petrol.*, 1998, **39**, 1847–1864.

ACKNOWLEDGEMENTS. N.R.K. thanks the Head, Department of Geology, University of Pune, Pune, for granting special permission to collaborate with GEMOC Macquarie University, Sydney, Australia. We thank Prof. W. L. Griffin and Prof. Suzanne O'Reilly for the collaboration as well as for the discussions. We are also grateful to Ms Carol Lawson and Dr Norm Pearson for their help in the Microprobe analysis and Mrs Ashwini Sharma for help in the ICPMS microprobe analysis. We thank Dr Mark Norman and the post-doctoral fellows at the Centre for fruitful discussions. Review comments from the anonymous referee(s) helped to improve the manuscript.

Received 13 August 2001; revised accepted 11 February 2002

A technique for quick estimation of aphid numbers in field

Abraham Verghese* and P. D. Kamala Jayanthi

Division of Entomology and Nematology, Indian Institute of Horticultural Research, Hesseraghatta Lake PO, Bangalore 560 089, India

Investigations were made to develop a quick method for *in situ* estimation of aphid numbers using *Aphis punicae* Passerini (Aphididae: Homoptera) on pomegranate as case study. Regression analysis was made between aphid number and length of infestation on the sampling unit, viz. fresh terminal shoots of pomegranate in three arbitrary infestation classes – heavy, medium and low. The study indicated that for reliable estimation of aphid numbers under high-density infestation, power ($y = 202.74x^{0.5358}$; $R^2 = 0.8244$) and linear ($y = 56.57x + 187.35$; $R^2 = 0.7496$) models were adequate. Under medium density infestation, linear ($y = 11.517x + 55.634$; $R^2 = 0.7093$) and power ($y = 34.129x^{0.7049}$; $R^2 = 0.8268$) models and under low-density infestation linear model ($y = 9.75x–8.7548$; $R^2 = 0.7767$) were found adequate. The models worked out in the present study can be used for quick sampling of aphid numbers under field conditions by grading the infestation and measuring the length of the infestation, and substituting the same in the above models.

APHIDS are interesting subjects for studying 'population dynamics'. However, their high reproductive rates and colonizing habits lead to high unit density, rendering field enumeration difficult. Precision recording of the aphid numbers is a prerequisite to several ecological investigations and other studies related to their management.

*For correspondence.

The distribution of aphids on most plants is aggregated typical of many insects[1]. In general, aphids prefer to feed and reproduce on young growing parts compared to mature parts[2]. Further, the aphids that aggregate set different problems from those that disperse. Aggregates of aphids are usually easier to find than widely spaced species, but it is more difficult to estimate their numbers. Hence, the present study was carried out for developing a method for *in situ* estimation of aphid numbers in case of *Aphis punicae* Passerini (Aphididae: Homoptera) colonizing pomegranate (*Punica granatum* L.) trees. The population of aphids within the plant ranges from low to high density on tender shoots[3]. Thus mixed type of infestation does occur in the same plant, warranting grading of infestation as low, medium and high. The pomegranate aphid is a serious pest on pomegranate and in any management or field evaluation, investigators require quick estimation of large samples. Therefore, the present study was carried out to arrive at an estimation model for precision field-estimation of aphid numbers.

The experiment was carried out in the pomegranate (cv. *Ganesha*) field of Indian Institute of Horticultural Research, Bangalore (12°58′N; 77°35′E) during 1999–2000 for the pomegranate aphid, *A. punicae*. The aphid infestation was classified into three classes, viz. heavy, medium and low. Heavy (H) means aphids present in large numbers with dense infestation on leaves and stems of new terminal shoots. Medium (M) means aphids present in large numbers in recognizable colonies but diffused, and infesting a large proportion of the leaves and stems, and low (L) refers to aphids present in small numbers but not in recognizable colonies and diffused. The sampling unit constituted terminal tender shoots (approximately 15 cm length) on which aphids selectively colonize. However, aphids tend to congregate more towards the terminal end and rarely to the base of the shoot. Twenty-five sampling units (terminal shoots) of each class were randomly taken and the infestation length (linear spread of aphid colony along shoot axis) was measured in centimetres with a scale. Next, the sample shoots were carefully cut and brought to the laboratory in individual sealed polythene bags to prevent any escape of aphids, and the actual numbers of aphids on the shoot were counted under a stereo binocular microscope. The data were tabulated and subjected to linear and nonlinear analyses for all the three categories, with length (x) as independent factor and mean number of aphid per shoot (y) as dependent factor. These relationships take the following forms of equation: Linear – $y = a + bx$; Logarithmic – $y = C \ln x + b$; Exponential – $y = C\, e^{bx}$; Power – $y = C\ x^b$; Polynomial – $y = b + C_1x + C_2x^2 + C_3x_3 \ldots C_nx^n$ (where y is the predicted mean population, x is the factor, a is the intercept ($a = y - bx$) and b is the slope; thus C, $C_1 \ldots C_n$ and b are constants, ln is the natural logarithm and e is the base of the natural logarithm). The coefficient of determination (R^2) reflects the extent to which